Ni-BASED NANOWIRE ARRAYS AS CHEMICAL AND MAGNETIC FIELD SENSORS

Adrian RADU [1], Sorina IFTIMIE [1], Lucian ION [1], Stefan ANTOHE [1, 2], Daniela DRAGOMAN [1, 2,]

[1] University of Bucharest, Physics Faculty, "Materials and Devices for Electronics and Optoelectronics" Research Center,
PO Box MG-11, 077125 Bucharest-Magurele, Romania
[2] Academy of Romanian Scientists, Splaiul Independentei 54, 050094, Bucharest, Romania
Corresponding author: Daniela DRAGOMAN, E-mail: `daniela@solid.fizica.unibuc.ro`

Abstract. Dense arrays of homogeneous Ni nanowires as well as segmented Ni/Cu nanowires were fabricated by electrochemical deposition in the nanopores of an alumina template. In order to highlight the wide application range of these nanowire arrays and the versatility of their fabrication method, we showed that homogeneous Ni nanowire arrays can be used as chemical sensors, while Ni/Cu segmented nanowire arrays act as magnetic fields detectors.

Key words: Ni nanowires, chemical sensor, magnetic field sensor.

1. INTRODUCTION

Nanostructured systems, in particular nanowires based on Ni or Ni alloys are suitable as sensors due to their magnetic properties [1, 2] and catalytic properties/chemical response [3–5] in the presence of certain substances, eventually after an appropriate functionalization of the surface. Both chemical and magnetic responses are strongly dependent on the dimensions, composition, shape, and morphology of nanowires.

Such sensors can consist of individually contacted or arrays of nanowires [2], the latter being generally grown by electrochemical deposition inside the nanopores of a template. This relatively low-cost growth method of nanowires does not require very sophisticated equipments and is very versatile, being suitable for fabricating either metallic or semiconducting nanowires with determined composition and diameters [6–9]. In addition, homogeneous or segmented nanowires can be obtained by controlling specific growth parameters [10–13].

In this paper we show that Ni and segmented Ni/Cu nanowire arrays, grown inside the nanopores of an alumina template, act as chemical and magnetic field sensors, respectively. The results reported in this paper demonstrate the wide range of applications of Ni-based nanowires fabricated by this versatile method.

2. FABRICATION OF THE ALUMINA TEMPLATE

The template is fabricated on a Si(111)/SiO$_2$ substrate (the SiO$_2$ width is 30 nm), cleaned by ultrasonication in a bath of benzene and acetone. The substrate is covered by DC cathodic pulverization with an Au film, which has a double role: as anodization barrier for the subsequent deposition of the Al film, and as working electrode in the electrochemical anodization and subsequent deposition of nanowires. The Al layer is then deposited also by DC cathodic pulverization. The anodization of the Al film was performed in a home-made electrochemical cell, which assures an optimum temperature control of the electrolytic bath. More specifically, the anodization temperature was kept constant, around 3–5 ^{o}C, to avoid the closure of nanopores. A three-electrode configuration was used, consisting of the two working electrodes and a commercial reference electrode from saturated calomel (SCE). The anodization electrolyte consists of a mixture of oxalic and phosphoric acids, the complete chemical reaction being:

$$2Al + 3H_2O \rightarrow Al_2O_3 + 3H_2. \tag{1}$$

The chrono-ampermetric curve recorded during anodization and presented in Fig. 1a reveals the three stages of the process: (i) formation of a thin Al_2O_3 layer at the cathode surface (Al film), associated to the initial sharp decrease of the current; (ii) balance reaching between the two competing processes: dissolution of the formed oxide in the region of intense electric field and continuation of the oxidation process, which lead to nanopore formation; and (iii) nanopore growth up to the Au electrode, which inhibits oxidation and is responsible for the sharp increase of the current due to the electrolyte short-circuit. The inset of Fig. 1a is a side-view of the alumina membrane with nanopores, the SEM image in Fig. 1b showing the resulting high-density nanopores in the membrane.
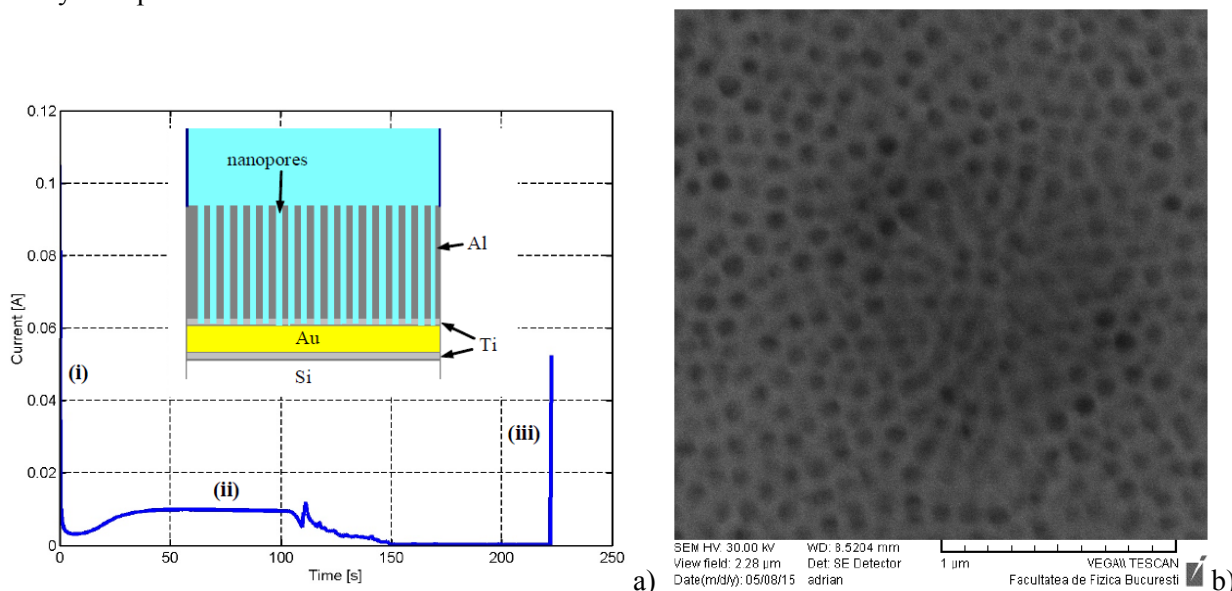

Fig. 1 – a) Chrono-ampermetric curve; b) SEM image of the porous alumina membrane.

The chrono-ampermetric curve recorded during anodization and presented in Fig. 1a reveals the three stages of the process: (i) formation of a thin Al_2O_3 layer at the cathode surface (Al film), associated to the initial sharp decrease of the current; (ii) balance reaching between the two competing processes: dissolution of the formed oxide in the region of intense electric field and continuation of the oxidation process, which lead to nanopore formation; and (iii) nanopore growth up to the Au electrode, which inhibits oxidation and is responsible for the sharp increase of the current due to the electrolyte short-circuit. The inset of Fig. 1a is a side-view of the alumina membrane with nanopores, the SEM image in Fig. 1b showing the resulting high-density nanopores in the membrane.

3. FABRICATION OF THE MATRIX OF NI NANOWIRES

The Ni nanowires were grown inside the pores of the alumina membrane by electrochemical deposition. More precisely, the Ni nanowires were obtained using as electrolyte a Watts bath containing 225 g/L of $NiSO_4·6H_2O$ and 30 g/L of $NiCl_2·6H_2O$. A PC driven VoltaLab potentiometer controlled the electrochemical process in the three-electrode configuration with an Au cathode, a Pt anode and a SCE reference electrode. The temperature was kept at 5 ^{o}C during the growth of Ni wires. Under these conditions, the reaction at the cathode is:

$$Ni^{2+} + 2e^- \rightarrow Ni^0. \tag{2}$$

After the pores are filled, the template membrane is dissolved in an alkaline solution of NaOH, so that the matrix of Ni nanowires remains exposed.

Figures 2a–c present SEM images with increasing magnification of the nanowire matrix grown on a set of Au interdigitated electrodes. As can be observed from these figures, the nanowires grow only on the metallic surfaces/electrodes. The average diameters and lengths of the nanowires are 90 nm and 700 nm, respectively.
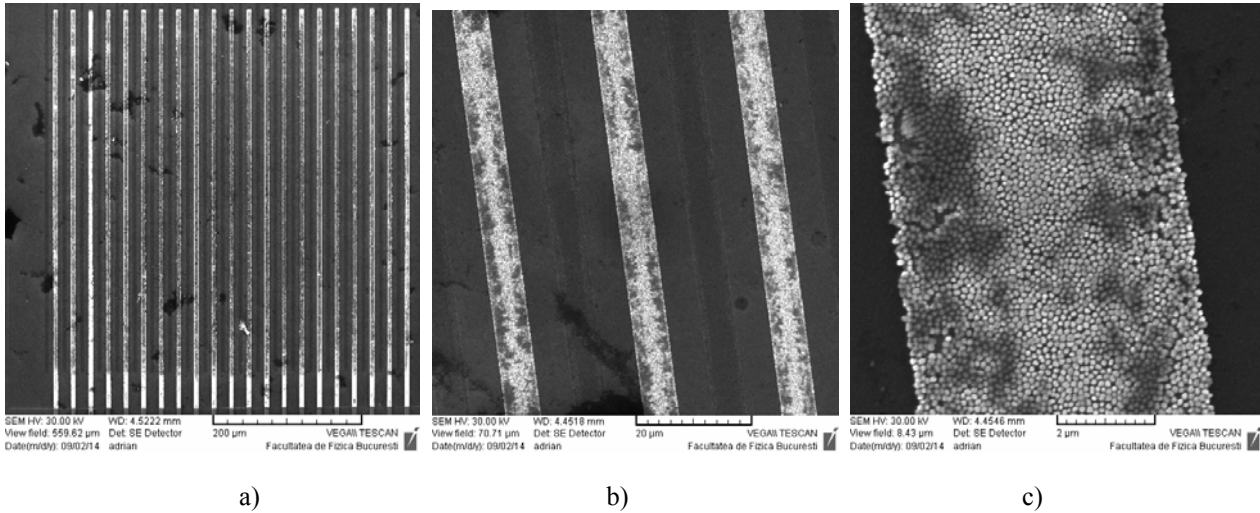
Fig. 2 – SEM images with increasing magnification of the nanowire array grown on Au interdigitated electrodes.

4. NI NANOWIRES AS GLUCOSE SENSORS

The interdigitated electrodes covered with Ni nanowires were then used as chemical sensor, for capacitive detection of glucose. The presence of Ni nanowires enhances the sensitivity of the sensor due to the increased surface/volume ratio as well as the high catalytic activity of Ni in the glucose oxidation process.

The capacitive response was determined by impedance spectroscopy, the capacitance being extracted from the real and imaginary parts of the measured output signal, denoted by X and Y, respectively, according to the formula:

$$ C = \frac{\sqrt{(V_g - X)^2 - Y^2}}{2\pi f R \sqrt{X^2 + Y^2}} \sin\left[\arctan\left(\frac{-Y}{V_g - X} \right) - \arctan\left(\frac{Y}{X} \right) \right], \tag{3} $$

where V_g is the input signal with frequency f.

The frequency dependences of X and Y of the capacitive detector are presented in Fig. 3(a) for different concentrations of glucose test solutions, the corresponding dependence of the capacitance, determined from (3), being illustrated in Fig. 3b. The lock-in detection system is represented in the inset of the last figure, the concentrations of the test solutions in g/l being indicated in the legend of Fig. 3b. Note that for glucose, with a molecular weight of 180.16 g/mol, 1 g/l is equivalent to 5.55 mM. The curves in Fig. 3 show that the output signal does not depend on frequency, at least for the f range in this study, and that the detector senses glucose concentrations as small as 50 μM. Although not focused on finding the detection limit of the Ni nanowire sensor, and not optimized for sensing purposes, the results of the study in Fig. 3 reveal that this capacitive sensor can detect any anomalies in the physiological level of glucose, the normal level of which is of 3–5 mM. Note that arrays of Pt/Ni nanowires with average diameters and widths of 200 nm and 4 μm, respectively, have a detection limit for glucose of about 2 μM, due partially to the catalytic activity of Pt, which is, however, a rare element [14]. From Fig. 3, as well as from Fig. 4, which presents the calibration curves of the detector in the range of the studied concentrations, at different frequencies, it follows that the response of the Ni nanowire capacitive sensor is not linearly dependent on the glucose concentration. This could be a consequence of the limited adsorbtion of glucose molecules on the surface of Ni nanowires in a high-density array caused by a limited diffusion of glucose molecules inside the array.

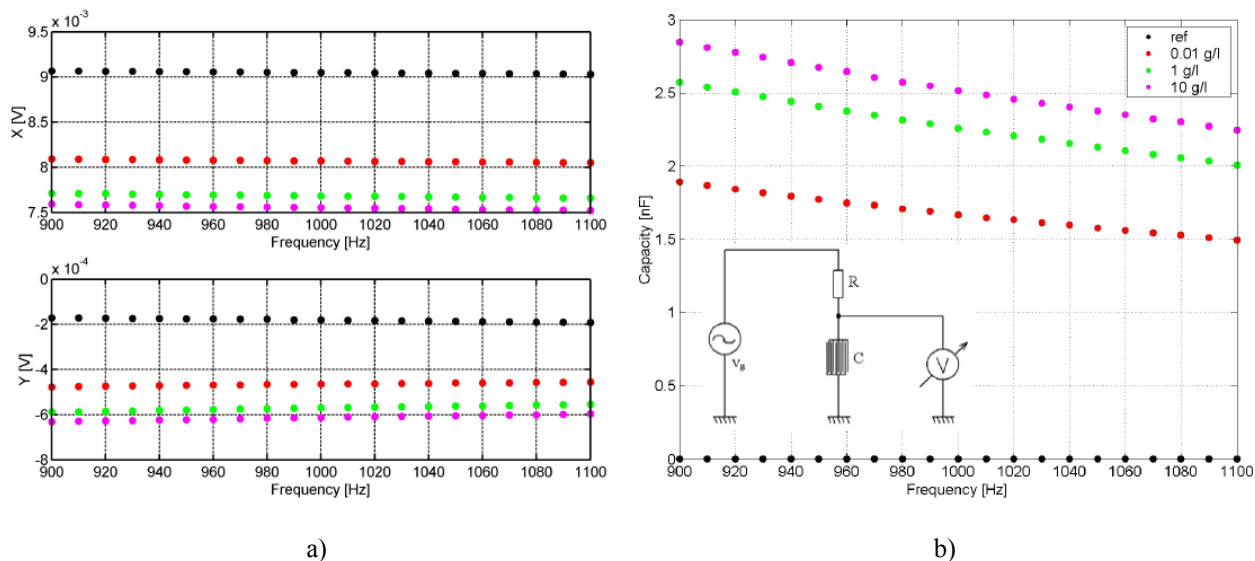a)   b)

Fig. 3 – Frequency dependences of: a) the real and imaginary parts of the output signal;
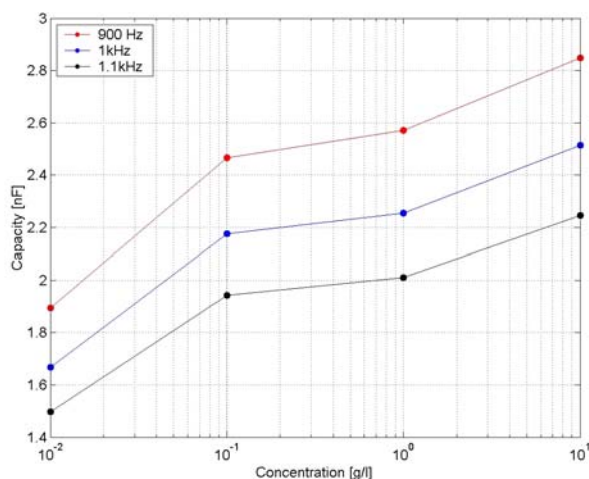b) capacitance for different test solution concentrations.

Fig. 4 – Calibration curves of the glucose detector in the range of the studied concentrations, at different frequencies.

5. FABRICATION OF THE NI/CU SEGMENTED NANOWIRE ARRAY

Arrays of Ni/Cu segmented nanowires have been also electrochemically deposited inside the pores of the alumina template. More precisely, the segmented nanowires were sequentially grown from a single electrolytic Watts-type bath containing a solution of $NiSO_4 \cdot 6H_2O$ (225 g/l), $NiCl_2 \cdot 6H_2O$ (30 g/l), boric acid (22.5 g/l) and hydrated copper sulphate (4 g/l), the growth control being assured by a stepwise variation of the electrode potential between the values that favor the deposition of a specific metal (Ni or Cu). Figure 5 presents the programmed sequence of applied pulses of the electrode potential (up) and the time-dependent deposition current (bottom). The sequence of pulses necessary to grow a Cu/Ni period of the segmented nanowire is 6.0 s at –120 mV (potential value that favors Cu deposition) and 0.5 s at –1100 mV (potential that favors Ni deposition). The SEM images with different magnifications of the resulted segmented Ni/Cu nanowires, with average diameter of about 90 nm, are represented in Figs. 6a–b, the different segments being clearly observed in the last image.
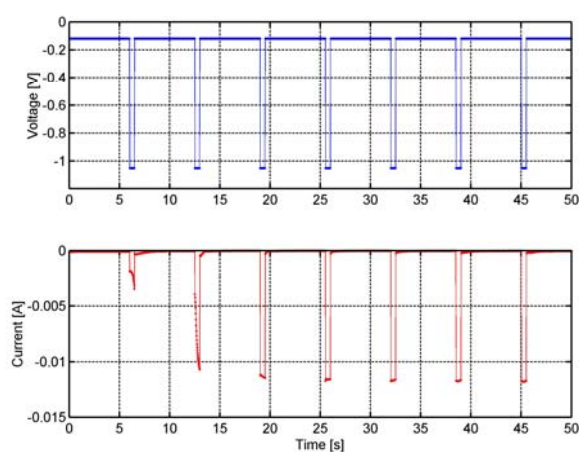
Fig. 5 – Programmed sequence of applied pulses of the electrode potential (up)
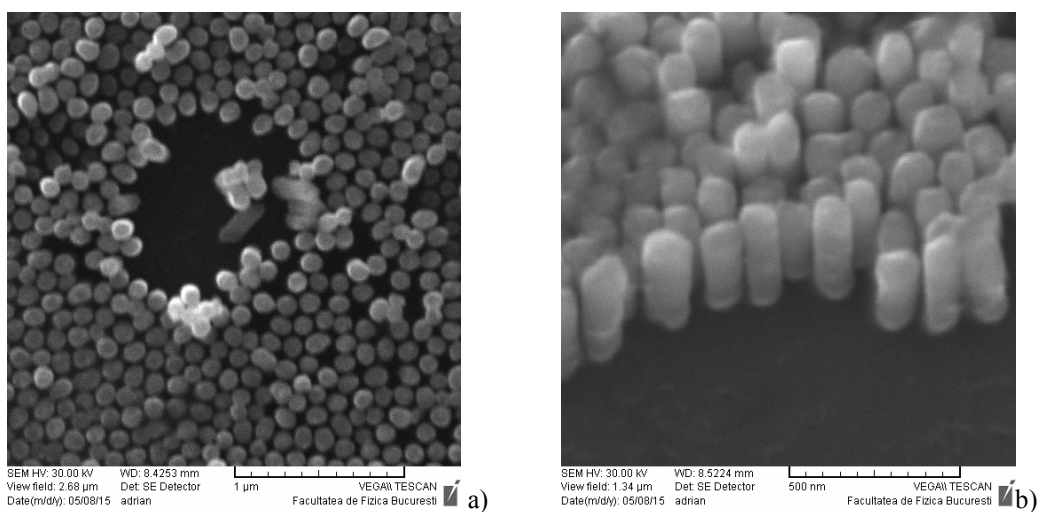and the time-dependent deposition current (bottom).

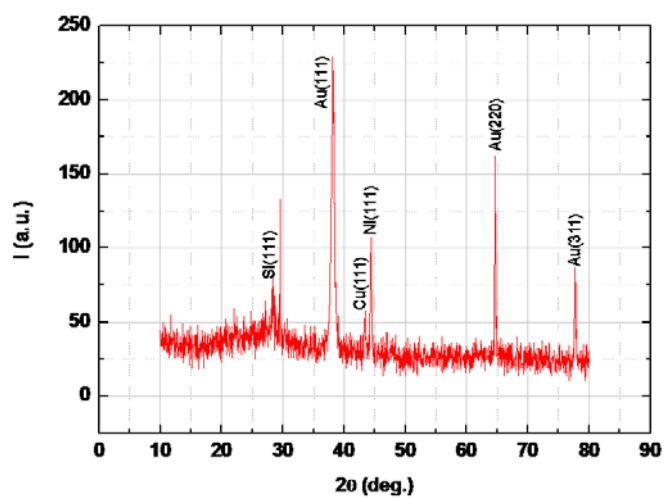Fig. 6 – SEM images with different magnifications of segmented Ni/Cu nanowires.

Fig. 7 – X-ray diffraction spectrum of segmented nanowires.

The X-ray diffraction spectrum in Fig. 7, obtained with a high-resolution diffractometer (Bruker D8 Discover) using the Cu-K$_{\alpha 1}$ radiation (λ = 1.5406 Å) in a grazing incidence configuration confirms the presence of both elements, Ni and Cu, in the nanowires. Diffraction peaks attributed to Au, which is the working electrode, and Si, which is the substrate, are also visible in the X-ray spectrum.

6. NI/CU SEGMENTED NANOWIRES AS MAGNETIC FIELD SENSORS

The magnetic response of Ni/Cu nanowires, in particular the dipolar interactions between magnetic layers and the magnetic shape anisotropy, can be tuned via the shape (rod-like versus disk-like) of the layers [15], the remanence, coercivity and Curie temperatures increasing with the length of the Ni segments [16].

We used segmented Ni/Cu nanowire arrays to detect magnetic fields via the magnetoresistive effect. To enhance the quality of the contact of the nanowire array, nanowires higher than the template were deposited, in order to form large-area metallic regions above the template. Figures 8a–b show the formation of such metallic clusters and, respectively, of a continuous metallic layer above the nanowire array, which can be used as electric contact. The insets in these figures are schematic side representations of the nanowire array in the pores of the template, as well as of the clusters/continuous layer above the template. The magenta (brown) segments correspond to Ni (Cu).
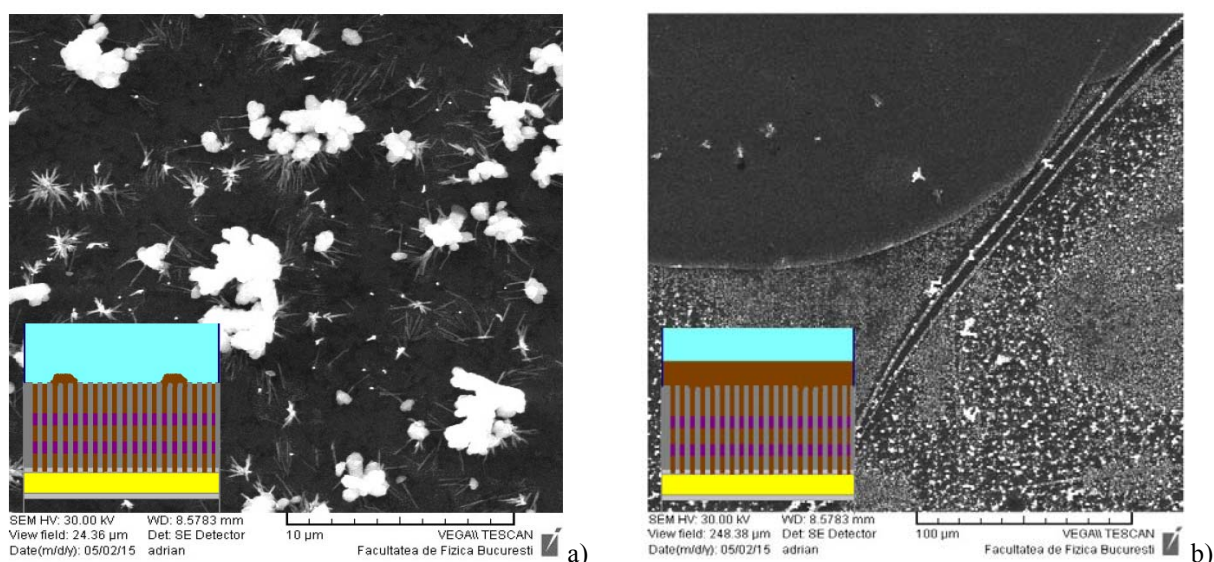

Fig. 8 – Formation of: a) metallic clusters; b) a continuous metallic layer above the nanowire array.

The electrical characterization of the segmented nanowire array revealed a linear dependence of the current on the applied voltage, the Ni/Cu interface having an ohmic behavior. The electrical resistance has small values, of few ohms, typical for metallic nanowires. The electrical resistance varies, however, in the presence of an applied magnetic field due to the magnetoresistive effect, decreasing from the value in the absence of the magnetic field with about 1.4 % for magnetic fields as low as 0.3 T. The magnetoresistive effect was observed also in other segmented nanowires containing ferromagnetic and diamagnetic materials grown by electrochemical deposition in the pores of a template [17, 18].

Further, we have studied the dependence of the transverse magnetoresistance on the length of the Ni/Cu period. The magnetoresistances of nanowires with a total length of about 700 nm containing 5 and, respectively, 10 Ni/Cu periods are represented in Figs. 9a and, correspondingly, 9b, as a function of the applied magnetic field. As expected, the magnetoresistance increases with the magnetic field, and is higher for the nanowire with smaller distances/enhanced interaction between Ni layers. Moreover, from Fig. 9 it follows that the magnetoresistance at room temperature is higher than at 200 K. In general, the magnetoresistance decreases with temperature, an opposite tendency being observed in individual Ni nanowires as well as in Ni nanowires in alumina templates, in which the magnetic anisotropy changes direction due to a temperature-induced stress caused by different thermal expansion coefficients of Ni and the surrounding media [19, 20]. This effect could also explain the results in Fig. 9.
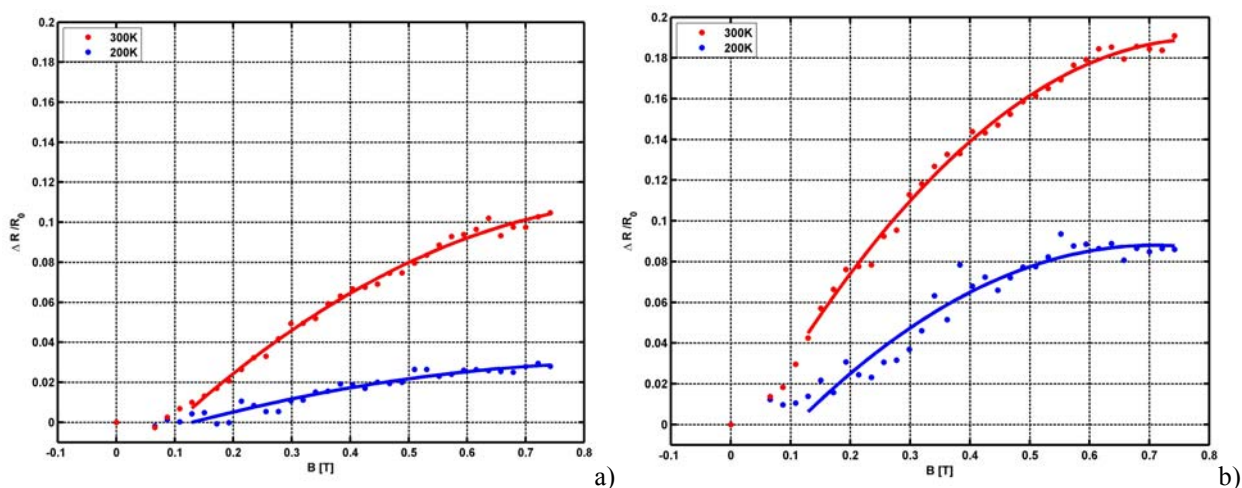
Fig. 9 Magnetoresistance dependence on the magnetic field for a segmented Ni/Cu nanowires array with:
a) 5; b) 10 periods.

7. CONCLUSIONS

We have demonstrated that Ni-based nanowire arrays fabricated by electrochemical deposition in the nanopores of an alumina template have a wide range of applications. Homogeneous Ni nanowire arrays grown via this versatile method could be used as chemical sensors, while Ni/Cu segmented nanowire arrays are able to detect magnetic fields. The results emphasize the potentialities of nanowire arrays fabricated by this adaptable method.

ACKNOWLEDGEMENTS

REFERENCES

1. B. YOO, Y. RHEEM, W.P. BEYERMANN, N.V. MYUNG, *Magnetically assembled 30 nm diameter nickel nanowire with ferromagnetic electrodes,* Nanotechnology, **17**, pp. 2512–2517, 2006.
2. V. VEGA, T. BÖHNERT, S. MARTENS, M. WALECZEK, J.M. MONTERO-MORENO, D. GÖRLITZ, V.M. PRIDA, K. NIELSCH, *Tuning the magnetic anisotropy of Co-Ni nanowires: comparison between single nanowires and nanowire arrays in hard-anodic aluminum oxide membranes*, Nanotechnology, **23**, 465709, 2012.
3. W. YAN, D. WANG, L.A. DIAZ, G.G. BOTTE, *Nickel nanowires as effective catalysts for urea electro-oxidation*, Electrochimica Acta, **134**, pp. 266–271, 2014.
4. C. DU, M. CHEN, W. WANG, G. YIN, *Nanoporous PdNi alloy nanowires as highly active catalysts for the electro-oxidation of formic acid,* ACS Appl. Mater. Interfaces, **3**, pp. 105–109, 2011.
5. X.K. TIAN, X.Y. ZHAO, L.D. ZHANG, C. YANG, Z.B. PI, S.X. ZHANG, *Performance of ethanol electro-oxidation on Ni-Cu alloy nanowires through composition modulation*, Nanotechnology, **19**, 215711, 2008.
6. D.D. LI, R.S. THOMSON, G. BERGMANN, J.G. LU, *Template-based synthesis and magnetic properties of cobalt nanotube arrays*, Adv. Mater., **20**, pp. 4575–4578, 2008.
7. H. MASUDA, K. FUKUDA, *Ordered metal nanohole arrays made by a two-step replication of honeycomb structures of anodic alumina*, Science, **268**, pp. 1466–1468, 1995.
8. C. TAZLAOANU, L. ION, I. ENCULESCU, M. SIMA, M. ENCULESCU, E. MATEI, R. NEUMANN, R. BAZAVAN, D. BAZAVAN, S. ANTOHE, *Transport properties of electrodeposited ZnO nanowires*, Physica E, **40**, pp. 2504–2507, 2008.

9. M. GHENESCU, L. ION, L. ENCULESCU, C. TAZLAOANU, V.A. ANTOHE, M. SIMA, M. ENCULESCU, E. MATEI, R. NEUMANN, O. GHENESCU, V. COVLEA, S. ANTOHE, *Electrical properties of electrodeposited CdS nanowires*, Physica E, **40**, pp. 2485–2488, 2008.

10. S.H. XU, G.T. FEI, X.G. ZHU, B. WANG, B. WU, L.D. ZHANG, *A facile and universal way to fabricate superlattice nanowire arrays*, Nanotechnology, **22**, 265602, 2011.

11. E. MATEI, L. ION, S. ANTOHE, R. NEUMANN, I. ENCULESCU, *Multisegment CdTe nanowire homojunction photodiode*, Nanotechnology, **21**, 105202, 2010.

12. V.A. ANTOHE, A. RADU, M. MÁTÉFI-TEMPFLI, A. ATTOUT, S. YUNUS, P. BERTRAND, C.A. DUTU, A. VLAD, S. MELINTE, S. MÁTÉFI-TEMPFLI, L. PIRAUX, *Nanowire-templated microelectrodes for high-sensitivity pH detection*, Appl. Phys. Lett., **94**, 073118, 2009.

13. E. MATEI, I. ENCULESCU, M.E. TOIMIL-MOLARES, A. LECA, C. GHICA, V. KUNCSER, *Magnetic configurations of Ni-Cu alloy nanowires obtained by the template method*, J. Nanopart. Res., **15**, 1863, 2013.

14. S.S. MAHSHID, S. MAHSHID, A. DOLATI, M. GHORBANI, L. YANG, S. LUO, Q. CAI, *Template-based electrodeposition of Pt/Ni nanowires and its catalytic activity towards glucose oxidation*, Electrochimica Acta, **58**, pp. 551–555, 2011.

15. M. CHEN, L. SUN, J.E. BONEVICH, D.H. REICH, C.L. CHIEN, P.C. SEARSON, *Tuning the response of magnetic suspensions*, Appl. Phys. Lett., **82**, pp. 3310–3312, 2003.

16. M. SUSANO, M.P. PROENCA, S. MORAES, C.T. SOUSA, J.P. ARAÚJO, *Tuning the magnetic properties of multisegmented Ni/Cu electrodeposited nanowires with controllable Ni lengths*, Nanotechnology, **27**, 335301, 2016.

17. X.-T. TANG, G.-C. WANG, M. SHIMA, *Perpendicular giant magnetoresistance of electrodeposited Co/Cu-multilayered nanowires in porous alumina templates*, J. Appl. Phys., **99**, 033906, 2006.

18. K.Y. KOK, C.M. HANGARTER, B. GOLDSMITH, I.K. NG, N.B. SAIDIN, N.V. MYUNG, *Synthesis and characterization of electrodeposited permalloy (Ni$_{80}$Fe$_{20}$)/Cu multilayered nanowires*, J. Magn. Magnetic Materials, **322**, pp. 3876–3881, 2010.

19. Y. RHEEM, B.-Y. YOO, W.P. BEYERMANN, N.V. MYUNG, *Magnetotransport studies of single nickel nanowires*, Nanotechnology, **18**, 015202, 2007.

20. D. NAVAS, K.R. PIROTA, P. MENDOZA ZELIS, D. VELAZQUEZ, C.A. ROSS, M. VAZQUEZ, *Effects of the magnetoelastic anisotropy in Ni nanowire arrays*, J. Appl. Phys., **103**, 07D523, 2008.